Journal of Sound and Vibration 596 (2025) 118747

Contents lists available at ScienceDirect

Journal of Sound and Vibration

journal homepage: www.elsevier.com/locate/jsvi

Nonlinear dynamics of wing-like structures using a momentum subspace-based Koiter-Newton reduction

Kautuk Sinha [a,*], Farbod Alijani [b], Wolf R. Krüger [a], Roeland De Breuker [c]

[a] German Aerospace Center, Institute of Aeroelasticity, Goettingen, 37073, Germany
[b] Delft University of Technology, Faculty of Mechanical, Maritime and Materials Engineering, 2628, CN, Delft, the Netherlands
[c] Delft University of Technology, Faculty of Aerospace Engineering, 2629, HS, Delft, the Netherlands

ARTICLE INFO

Keywords:
Nonlinear dynamics
Reduced order models
Cantilevers
Aircraft wing

ABSTRACT

Cantilevers find a wide range of applications in the design of scientific equipment and large-scale engineering structures such as aircraft wings. Analysis techniques based on linearization approximations are unable to capture the large amplitude oscillation behaviour of such structures and thus, necessitates development of dedicated nonlinear methods. In this work, the recent developments in the Koiter-Newton model reduction method are utilized to obtain nonlinear reduced order models (ROMs) from full finite element structural models in order to simulate large amplitude dynamics of cantilevers. The method describes a nonlinear system of governing equations comprising quadratic and cubic terms which are obtained as higher order derivatives of the in-plane strain energy. To ensure that the large rotations in cantilevers and the resultant foreshortening effect is also accounted for, a ROM updating algorithm is adopted where the ROM parameters are varied with the structural deflections. Linear eigenmodes of the structure are utilized to form the reduction subspace. To validate the methodology, the ROM solution is compared against experimental results and a convergence study is conducted to identify the number of modes needed to replicate the nonlinear response. Finally, a composite wingbox structure is considered for which time domain simulations are conducted and frequency response curves, obtained through a frequency sweep, are presented.

1. Introduction

The utilization of cantilever structures is widespread in several engineering disciplines and is commonly observable in civil, mechanical and aerospace structures. The ability of cantilevers to deflect unrestricted on one end introduces unique characteristics into its kinematic behaviour. Unlike double-clamped structures, which tend to predominantly undergo elastic deformation under large loads, cantilever motion can be described as a combination of large rotations and elastic bending. At relatively large deflections and rotations, a nonlinear load-deflection behaviour is observable arising from geometric stiffening, follower forces and change of moment arm [1]. This implies that the solutions based on the linear theory have a limited application and cannot be applied correctly beyond a certain range of deflections.

Analytical models for nonlinear deflection in simple cantilever beams have been previously extensively studied. It has been highlighted in [1] that formulations for nonlinear curvature and corrections factors for the changing moment must be accounted for in

* Corresponding author at: German Aerospace Center, Institute of Aeroelasticity, Goettingen, 37073, Germany.
E-mail address: Kautuk.sinha@dlr.de (K. Sinha).

https://doi.org/10.1016/j.jsv.2024.118747
Received 11 January 2024; Received in revised form 23 July 2024; Accepted 17 September 2024
Available online 21 September 2024

order to predict the nonlinear behaviour of cantilevers. Early investigations on non-planar cantilever dynamics using inextensibility constraints have also shown that the nonlinear curvature effects have a significant influence on the motion of the system [2,3]. The inextensible beam however, has applications limited to cases where the cross-section area is much smaller than the beam length [4,5] and therefore, it can be assumed that shear deformation does not have any noteworthy effect. The so called geometrically exact model, where no approximations are made with respect to the kinematics of the system, provides a generic description of the nonlinear behaviour of cantilevers. Variants of this model have been commonly utilized for nonlinear static and dynamic investigations of cantilevers [6-10]. When modelling aircraft wings for nonlinear analyses, it has recently been common practice to develop low order models in the form of equivalent beams which approximate the wing deflection behaviour and subsequently, utilize the geometrically exact models [11-15]. In nonlinear dynamic investigations, the benefits gained through reduced order models (ROMs) are well known [16-19]. Development of ROMs based on analytical methods for complex models however, may require a large number of degrees of freedom to obtain a converged response [20].

Alternatively, ROMs based on numerical formulations have been derived directly from finite element (FE) models which obviously offer more flexibility in terms of the complexity of the analysed structure. These methods, in general, can be classified as intrusive and non-intrusive methods. The intrusive methods explicitly consider nonlinear stiffness coefficients within the FE formulation. The non-intrusive methods are necessary when it is not possible to obtain the nonlinear coefficients directly. This can be achieved by imposing specified displacement fields on a structural model and computing the restoring force from a set of nonlinear static FE analyses. A set of equations are then obtained in the generalized coordinates, the solution of which provides the unknown nonlinear stiffness coefficients [21]. Alternatively, a similar method to evaluate nonlinear coefficients using regression analysis with the application of prescribed static loads to a finite element model is discussed in [22]. Another family of ROMs based on utilization of mode derivatives has been extensively investigated. A method based on the reduction subspace enrichment using modal derivatives was first proposed in [23] where the finite element discretization is used as starting point. A method for selecting the most relevant second order modal derivatives was proposed in [24]. Modal derivatives have been further utilized in [25] where time domain simulations were conducted on an aircraft wing model. However, it is also highlighted that the reduction basis can rapidly increase in size for large models. The extended modal approach [26] specifically focusses on the utilization of higher order mode derivatives to account for the foreshortening effect in modelling moderately large deflection of aircraft wings. Invariant manifold techniques have also been utilized for studying nonlinear dynamics of a rotating beam [27] and an aircraft wing comprising large number of degrees of freedom [28]. The Koiter-Newton (K-N) model reduction [29-30] is another technique where the ROM is derived from an FE model. The approach considers nonlinear stiffness in the intrusive form i.e. nonlinear terms in the governing equations are directly obtained from FE formulations. The method was originally developed for post-buckling analyses and was subsequently utilized to investigate nonlinear dynamics using a momentum subspace formulation [31]. The K-N reduction was later extended to the study of nonlinear static deflections in a cantilevered wingbox structure [32]. It was also demonstrated that due to the large rotation effects in cantilevers, the ROM based on K-N reduction has a limited range of validity.

The work presented in this article aims to exploit the recent developments in the K-N reduction approach and investigate the nonlinear dynamics of wing-like structures. Analogous to the preliminary static results seen in [32], ROM based on the K-N reduction in the unloaded state of the structure is unable to capture the nonlinear dynamics at large deflections. To resolve this issue, a ROM updating strategy within the framework of the Newmark time integration [33] scheme has been developed which enables us to simulate large amplitude dynamics of cantilevers. The approach does not make use of the common enforced inextensibility condition but rather relies on finite element-based formulations and generation of a ROM that varies with the structural deflections. The novel contributions of this work include the first investigations of nonlinear dynamics of cantilevers using the K-N reduction along with a modelling strategy to improve the ROM performance for extremely large amplitude dynamic response. The approach is validated against finite element simulations and experimentally generated frequency response curves. Finally, the method is applied to generate nonlinear frequency response curves of a composite wing box assembly comprising 24,582 degrees of freedom.

The remainder of the article is divided into the following sections: Section 2 discusses the theoretical formulation of the momentum subspace-based K-N reduction, Section 3 discusses the ROM updating strategy within Newmark time integration, and finally, in Section 4 the test cases are presented along with relevant discussions.

2. Theoretical formulation

The equations utilized for the ROM formulation based on the Koiter-Newton reduction is summarized in this section. A detailed description of the formulations for nonlinear statics and nonlinear dynamics can be found in [29-31]. We first present the ROM equations as derived in their original form for nonlinear static analyses. Thereafter, the adaptations made for the nonlinear dynamic formulation are discussed.

Under static loading conditions, the internal forces in a structure are a function of its displacements $\mathbf{f}_{\text{int}} = \mathrm{f}(\mathbf{u})$ which can be expanded in the Taylor series about an equilibrium position. For a full FE model, where **L, Q, C** are the linear, quadratic and cubic stiffness tensors respectively, the internal force is described as:

$$\mathbf{f}_{\text{int}} = \mathbf{Lu} + \mathbf{Quu} + \mathbf{Cuuu} + O(\|\mathbf{u}\|^4) \tag{1}$$

It is assumed that a linear subspace of the force space exists and can be parameterized by coordinates $\boldsymbol{\phi}$**.** The force subspace **f** is then described as:

$$\mathbf{f} = \mathbf{F}\boldsymbol{\phi} \tag{2}$$

where $\mathbf{F}$ is a load matrix and comprises the external load and additional perturbation load vectors $\mathbf{f}_\alpha$. At equilibrium then $\mathbf{f} = \mathbf{f}_{\text{int}}$ must be satisfied.

Analogous to Eq. (1), the internal force $\boldsymbol{\phi}_{\text{int}}$ in the ROM subspace is described as:

$$\boldsymbol{\phi}_{\text{int}} = \overline{\mathbf{L}}\boldsymbol{\xi} + \overline{\mathbf{Q}}\boldsymbol{\xi}\boldsymbol{\xi} + \overline{\mathbf{C}}\boldsymbol{\xi}\boldsymbol{\xi}\boldsymbol{\xi} + O\left(\|\boldsymbol{\xi}\|^4\right) \tag{3}$$

where $\overline{\mathbf{L}}$, $\overline{\mathbf{Q}}$, $\overline{\mathbf{C}}$ are the linear, quadratic and cubic stiffness tensors of the ROM and $\boldsymbol{\xi}$ is the generalized displacement in the ROM subspace.

The equilibrium solution $\mathbf{u}$ is parameterized by the generalized displacement $\boldsymbol{\xi}$ and approximated using the Taylor series expansion as:

$$\mathbf{u}(\boldsymbol{\xi}) = \mathbf{u}_\alpha\boldsymbol{\xi} + \mathbf{u}_{\alpha\beta}\boldsymbol{\xi}\boldsymbol{\xi} + \mathbf{u}_{\alpha\beta\gamma}\boldsymbol{\xi}\boldsymbol{\xi}\boldsymbol{\xi} + O\left(\|\boldsymbol{\xi}\|^3\right) \tag{4}$$

where $\mathbf{u}_\alpha$, $\mathbf{u}_{\alpha\beta}$, $\mathbf{u}_{\alpha\beta\gamma}$ are the first, second and third order displacement fields, respectively. This parameterization is fixed by choosing $\boldsymbol{\xi}$ to be a work conjugate of $\boldsymbol{\phi}$, as given by:

$$(\mathbf{F}\boldsymbol{\phi})'\delta\mathbf{u} = \boldsymbol{\phi}'\delta\boldsymbol{\xi} \tag{5}$$

Substituting Eq. (4) into left hand side of Eq. (5) and solving for the coefficients, a set of constraint equations are obtained. The constraint equations are defined as:

$$\mathbf{f}'_\alpha\,\mathbf{u}_\beta = \delta_{\alpha\beta},\ \mathbf{f}'_\alpha\,\mathbf{u}_{\beta\gamma} = 0,\ \mathbf{f}'_\alpha\,\mathbf{u}_{\beta\gamma\delta} = 0 \tag{6}$$

where $\delta_{\alpha\beta}$ is the Kronecker delta. The constraint equations imply that the component vectors $\mathbf{f}_\alpha$ of the force subspace are orthogonal to the higher order displacement fields.

Combining Eq. (1-4) and solving for the coefficients of the various powers of $\boldsymbol{\xi}$ terms, we obtain three sets of linear equations. The orthogonality constraints obtained in Eq. (6) are appended to these equations. Together, these equations can be written in the matrix form and utilized for evaluation of the ROM parameters:

$$\begin{bmatrix} \mathbf{L} & -\mathbf{F} \\ -\mathbf{F}' & 0 \end{bmatrix} \begin{Bmatrix} \mathbf{u}_\alpha \\ \overline{\mathbf{L}}_\alpha \end{Bmatrix} = \begin{Bmatrix} 0 \\ -\mathbf{E}_\alpha \end{Bmatrix} \tag{7}$$

$$\begin{bmatrix} \mathbf{L} & -\mathbf{F} \\ -\mathbf{F}' & 0 \end{bmatrix} \begin{Bmatrix} \mathbf{u}_{\alpha\beta} \\ \overline{\mathbf{Q}}_{\alpha\beta} \end{Bmatrix} = \begin{Bmatrix} -\mathbf{Q}(\mathbf{u}_\alpha, \mathbf{u}_\beta) \\ 0 \end{Bmatrix} \tag{8}$$

$$\overline{\mathbf{C}}_{\alpha\beta\gamma\delta} = \mathbf{C}(\mathbf{u}_\alpha,\ \mathbf{u}_\beta,\ \mathbf{u}_\gamma,\ \mathbf{u}_\delta) - \frac{2}{3}\left[\mathbf{u}'_{\alpha\beta}\,\mathbf{L}\,\mathbf{u}_{\delta\gamma} + \mathbf{u}'_{\beta\gamma}\,\mathbf{L}\,\mathbf{u}_{\delta\alpha} + \mathbf{u}'_{\gamma\alpha}\,\mathbf{L}\,\mathbf{u}_{\delta\beta}\right] \tag{9}$$

The subscripts $\alpha,\ \beta,\ \gamma,\ \delta$ vary over the range 1 to m, where m is the number of vectors in the load matrix, $\mathbf{E}_\alpha$ is a unit vector whose α^{th} term is 1 and all other terms are zero. The coefficients $\mathbf{u}_\alpha$ and $\mathbf{u}_{\alpha\beta}$ from the displacement parameterization in Eq. (4) are obtained as by-products of the ROM parameters and do not require an assumption beforehand. The displacement solution is reconstructed by considering only up to the second order terms in the displacement expansion.

The above set of Eq. (7-9) are obtained by considering the force subspace. It has been shown in [31] that the ROM formulation is extendable to dynamics through the use of D'Alembert's principle and a set of equations fully analogous to Eq. (7-9) are obtainable when formulating the ROM in the momentum subspace. Furthermore, as shown in [31], the utilization of the momentum subspace enables us to compute reduced mass and damping matrices which are required in the nonlinear dynamic formulations.

To adapt the ROM for nonlinear dynamics, a linear assumption for the momentum $\mathbf{p}$ of the full FE model is made in the momentum subspace:

$$\mathbf{p} = \mathbf{P}\boldsymbol{\pi} \tag{10}$$

where $\mathbf{P}$ is the reduction basis matrix formed as a product of the mass matrix and the modal matrix comprising m selected linear eigenvectors, and $\boldsymbol{\pi}$ is a vector of momentum amplitudes in the ROM subspace. The number of eigenvectors selected here determines the size of the ROM. The similarity in the form of Eq. (10) and Eq. (2) implies that a set of orthogonality constraint equations similar to Eq. (6) are obtained. The resulting set of ROM equations are subsequently modified only to the extent of replacing the load matrix $\mathbf{F}$ by the basis matrix $\mathbf{P}$ in the Eq. (7-8).

The ROM parameters using the momentum subspace are therefore, computed using the following equations:

$$\begin{bmatrix} \mathbf{L} & -\mathbf{P} \\ -\mathbf{P}' & 0 \end{bmatrix} \begin{Bmatrix} \mathbf{u}_\alpha \\ \overline{\mathbf{L}}_\alpha \end{Bmatrix} = \begin{Bmatrix} 0 \\ -\mathbf{E}_\alpha \end{Bmatrix} \tag{11}$$

$$\begin{bmatrix} \mathbf{L} & -\mathbf{P} \\ -\mathbf{P}' & 0 \end{bmatrix} \begin{Bmatrix} \mathbf{u}_{\alpha\beta} \\ \overline{\mathbf{Q}}_{\alpha\beta} \end{Bmatrix} = \begin{Bmatrix} -\mathbf{Q}(\mathbf{u}_\alpha, \mathbf{u}_\beta) \\ 0 \end{Bmatrix} \tag{12}$$

$$\overline{\mathbf{C}}_{\alpha\beta\gamma\delta} = \mathbf{C}(\mathbf{u}_\alpha,\ \mathbf{u}_\beta,\ \mathbf{u}_\gamma,\ \mathbf{u}_\delta) - \frac{2}{3}\left[\mathbf{u}'_{\alpha\beta}\ \mathbf{L}\ \mathbf{u}_{\delta\gamma} + \mathbf{u}'_{\beta\gamma}\ \mathbf{L}\ \mathbf{u}_{\delta\alpha} + \mathbf{u}'_{\gamma\alpha}\ \mathbf{L}\ \mathbf{u}_{\delta\beta}\right] \tag{13}$$

The inputs from the full FE model i.e. **L, Q, C**, that are required to compute the ROM parameters are obtained using a strain energy-based approach where the nonlinear strain definition is based on the Green-Lagrange strains [31]. The higher order derivatives of the strain energy provide the equations for internal forces and the required stiffness tensors.

Furthermore, the reduced mass matrix $\overline{\mathbf{M}}$ is evaluated using the modal matrix $\boldsymbol{\varphi}$ and the mass matrix of the full FE model **M**:

$$\overline{\mathbf{M}} = (\boldsymbol{\varphi}'\mathbf{M}\,\boldsymbol{\varphi})^{-1} \tag{14}$$

A quadratic damping model is also assumed and the damping matrix **D** of the FE model is defined proportional to the mass and stiffness matrices according to the well-known Rayleigh damping. The reduced damping matrix $\overline{\mathbf{D}}$ is evaluated using the following equation:

$$\overline{\mathbf{D}} = \overline{\mathbf{M}}(\mathbf{P}'\ \mathbf{M}^{-1}\ \mathbf{D}\ \mathbf{M}^{-1}\mathbf{P})\overline{\mathbf{M}} \tag{15}$$

In a more specific case, when mass proportional damping is utilized, Eq. (15) can be simplified to $\overline{\mathbf{D}} = \alpha\overline{\mathbf{M}}$ where α is the mass coefficient in Rayleigh damping.

Finally, the reduced force vector can be computed from the external force vector $\mathbf{f}_{\text{ext}}$ using the work equivalence conditions and is described by:

$$\boldsymbol{\phi} = \mathbf{u}'_\alpha\ \mathbf{f}_{\text{ext}} \tag{16}$$

The equation of motion for the ROM is then defined as:

$$\overline{\mathbf{M}}\,\ddot{\boldsymbol{\xi}} + \overline{\mathbf{D}}\,\dot{\boldsymbol{\xi}} + \overline{\mathbf{L}}\,\boldsymbol{\xi} + \overline{\mathbf{Q}}\,\boldsymbol{\xi}\boldsymbol{\xi} + \overline{\mathbf{C}}\,\boldsymbol{\xi}\boldsymbol{\xi}\boldsymbol{\xi} = \boldsymbol{\phi}(\mathrm{t}) \tag{17}$$

where the dot accent represent time derivative of the variables.

The reduced mass and damping matrices are in general dependent on the reduction subspace, as defined in Eq. (14) & (15). When the ROM is reformulated in a deformed state, the reduction subspace is also reconstructed. Only in the special case that the reduction subspace consists of mass orthonormalized eigenvectors, the reduced mass matrix is always normalized to an identity matrix. Any other choice of vectors in the reduction subspace would result in a varying reduced mass matrix. Besides, explicit accountability of nonlinear inertia terms usually arises due to certain approximations in the formulations. The commonly used beam inextensibility conditions, for example in [40], are known to introduce such nonlinear inertia terms in governing equations. In our formulation, such constraints have not been enforced.

It is to be noted that the choice of eigenmodes in the reduction subspace has a direct influence on the dynamic response analysis. For example, we cannot correctly analyse the second bending behaviour without including the second eigenmode shape in the reduction subspace. The ROM formulated for a range of frequencies then must also include all of the eigenmode shapes in the reduction subspace that are intended to be investigated.

All ROM parameters can be determined using Eq. (11-17). The computation procedure of full FE tensors required in order to derive these ROM parameters is summarized in the Appendix. In the following section, the solution methodology adapted is presented.

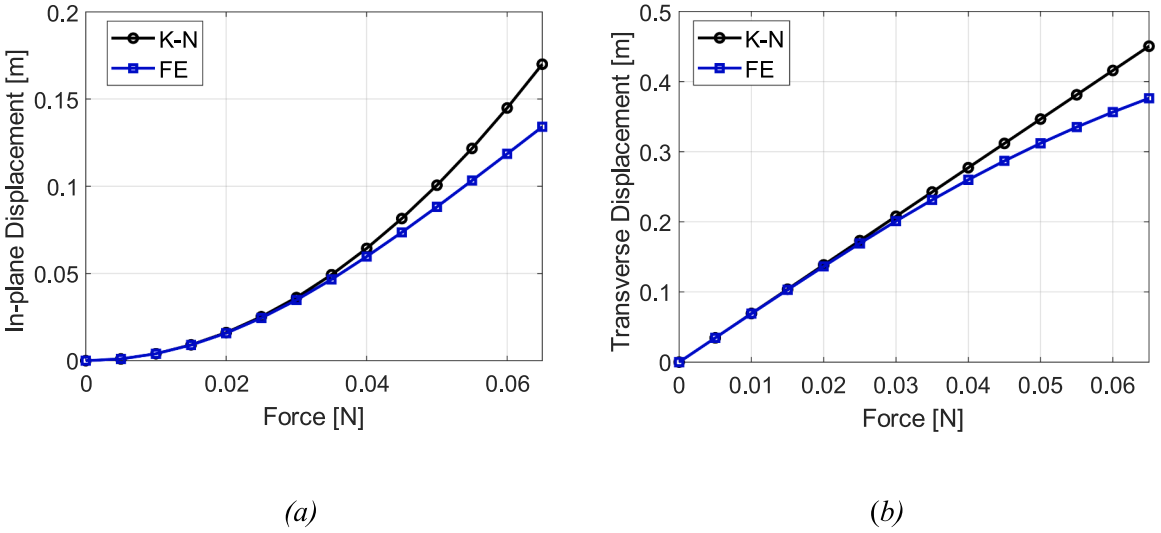

Fig 1. Peak displacements in steady state solutions of a steel cantilever beam of length $l = 0.6931$ m, $b = 0.0254$ m, $d = 0.99$ mm compared at different load amplitudes – (a) in-plane displacements, (b) transverse displacements.

3. Solution methodology

3.1. ROM updating procedure

To understand the extent of applicability of the K-N reduction, initial investigations are conducted on a cantilever beam whose geometrical and material properties were obtained from [34]. The dimensions of the beam are: length $l = 0.6931$ m, cross-section width $b = 0.0254$ m, cross-section depth $d = 0.99$ mm. The material properties of the beam are: elastic modulus $E = 200$ GPa, and density $\rho = 7{,}800$ kg/m^3. The cantilever tip is excited at the first modal frequency of 1.68 Hz and the applied force is incremented in steps. The ROM is formulated once at the initial undeformed configuration. A snapshot of the peak amplitude is captured at each loading step after the steady state response has been reached. These amplitudes are compared to corresponding full FE solutions obtained from MSC Nastran. It is evident from the comparisons in Fig. 1 that the ROM can closely replicate the full FE solution for a limited range of deflections, in this case up to 0.03 N load, while beyond that the error progressively increases.

In an earlier work, the K-N reduction was utilized for studying nonlinear static deflection of cantilever beams [32]. It was highlighted that the ROM computed in the initial undeformed shape of a cantilevered structure is insufficient to capture the complete load-deflection trajectory, especially at larger deflection amplitudes. It was demonstrated in the static case that an incremental ROM updating procedure coupled with a corrector step based on the Newton-Raphson iterations could improve the solution accuracy. In this method, the ROM parameters generated in one step are retained until the differences between the external and internal forces do not exceed a user-defined tolerance level. Beyond that, the geometry is deformed and updated and the relevant ROM parameters are regenerated.

The corrector step requires solving for full FE matrices and therefore, negates the benefits of the ROM, especially for large structural models. Executing the same procedure in time domain inevitably exponentially increases the simulation time. To truly gain the benefits of utilizing the ROM in dynamic analyses, it is imperative that a solution is obtained purely through the use of the ROM parameters. One of the objectives of this work is to understand if the ROM performance could be potentially improved for larger deflections under dynamic loading and for this purpose a ROM updating algorithm in combination with the Newmark time integration scheme is proposed.

Fig. 2 is a representation of the flow diagram of the ROM generation and the updating process in the nonlinear dynamics model. The computations begin with a preparatory offline stage where a nonlinear static analysis is conducted to assess the validity of the ROM, generate ROM parameters and determine displacement limits for which the ROM parameters hold validity. This implies that the region of ROM validity is predetermined based on the nonlinear static deflection profile. The ROM is then stored in a database and carried over to the dynamic analysis module where Eq. (1) is solved using the implicit form of the Newmark time integration. The original algorithm is modified to introduce the dependency of the ROM parameters on displacement limits. For clarity, the algorithm for the dynamic module is defined below in text form.

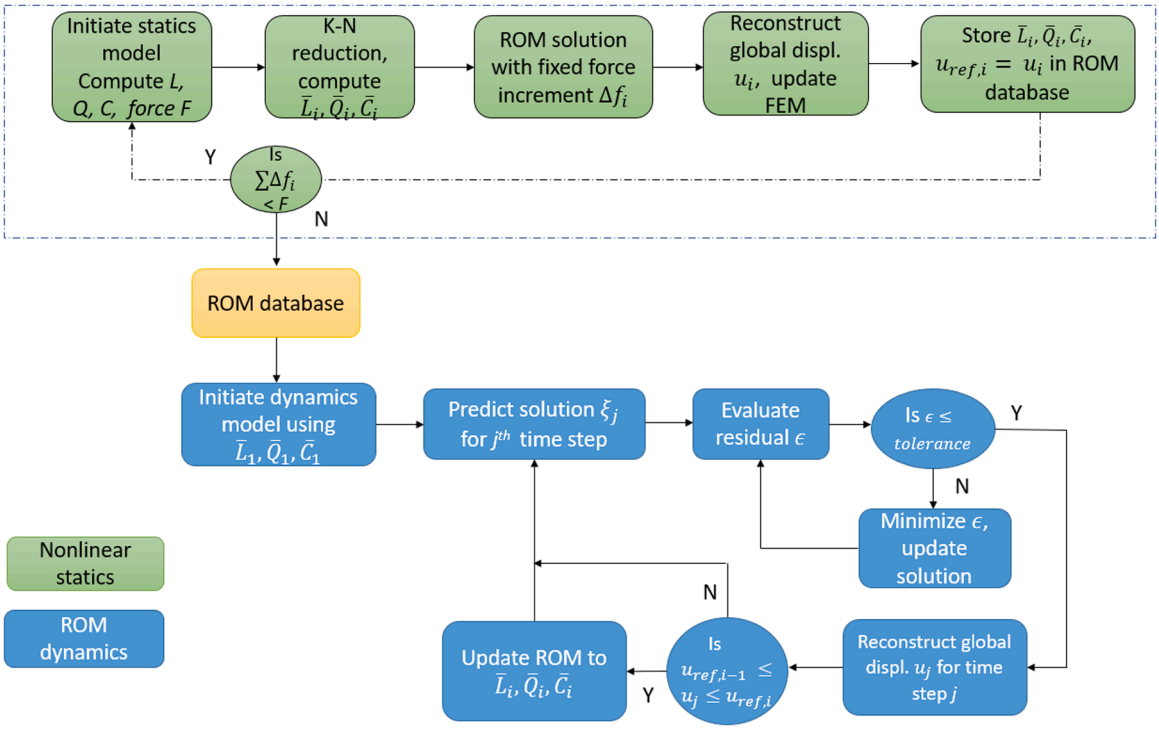

Fig 2. Algorithm for the K-N reduction and updating procedure.

Step 1: Select ROM parameters in the initial undeformed state of the structure. Initialize reference (undeformed) solution in the ROM subspace $\boldsymbol{\xi}_{\text{ref}} = 0$

Step 2: Obtain a solution predictor for the $j+1$th time step using the Newmark-beta method.

$$\ddot{\boldsymbol{\xi}}_{j+1} = 0;\ \boldsymbol{\xi}_{j+1} = \boldsymbol{\xi}_{\text{j}} + \dot{\boldsymbol{\xi}}_{\text{j}}\,\Delta t + \ddot{\boldsymbol{\xi}}_{\text{j}}\left(\frac{1}{2} - \beta\right)\Delta t^2;\ \dot{\boldsymbol{\xi}}_{j+1} = \dot{\boldsymbol{\xi}}_{\text{j}} + (1-\gamma)\ddot{\boldsymbol{\xi}}_{\text{j}}\,\Delta t$$

Step 3: Evaluate the force residual $\varepsilon = \| \boldsymbol{\phi}_{\text{in dyn}} - \boldsymbol{\phi} \|$ where $\boldsymbol{\phi}_{\text{in dyn}}$ is the internal force in the dynamic model.

Step 4: While $\varepsilon \geq$ tolerance:

$$\boldsymbol{\delta} = \boldsymbol{\xi}_{j+1} - \boldsymbol{\xi}_{\text{ref}}$$

$$\Delta\boldsymbol{\xi} = \left[\frac{\overline{\mathbf{M}}}{\beta\,\Delta t^2} + \frac{\gamma\overline{\mathbf{D}}}{\beta\,\Delta t} + \overline{\mathbf{L}} + \overline{\mathbf{Q}}\,\boldsymbol{\delta} + \overline{\mathbf{C}}\,\boldsymbol{\delta}\boldsymbol{\delta}\right]^{-1}\varepsilon$$

$$\boldsymbol{\xi}_{j+1} = \boldsymbol{\xi}_{j+1} + \Delta\boldsymbol{\xi},\ \dot{\boldsymbol{\xi}}_{j+1} = \dot{\boldsymbol{\xi}}_{j+1} + \frac{\gamma\,\Delta\boldsymbol{\xi}}{\beta\,\Delta t},\ \ddot{\boldsymbol{\xi}}_{j+1} = \ddot{\boldsymbol{\xi}}_{j+1} + \frac{\Delta\boldsymbol{\xi}}{\beta\,\Delta t^2}$$

Step 5: Convert the generalized displacements to real displacements using Eq. (4).

Step 6: Update ROM parameters if displacement limits are exceeded and update the reference configuration to the corresponding equilibrium solution. Update reference solution in the ROM subspace: $\boldsymbol{\xi}_{\text{ref}} = \boldsymbol{\xi}_{j+1}$

Step 7: Start solution for the next time step if $t \leq t_{max}$ (total simulation time).

The variables are always referred back to the previous reference equilibrium step and therefore, it is necessary to update the reference each time the ROM is updated. The parameters β and γ are set to 0.25 and 0.5 respectively for the unconditionally stable implicit Newmark algorithm [33].

3.2. Key considerations

- The procedure described in Section 3.1 relies on developing a ROM database through nonlinear static analyses. The extent of deflection in the nonlinear static case determines the range of validity of the ROM for dynamic analyses. For a generic test case and loading condition, prior information about the dynamic response is often unavailable. Therefore, it is practical to create a ROM database with sufficiently large loading conditions. For example, a wing of a transport aircraft is, by design, always expected to have tip deflections considerably lesser than 50 % of the span. Therefore, a ROM database created for up to 50 % tip deflection under static loading encompasses the entire operational range.
- For all loading conditions resulting in similar dynamic motion it is sufficient to utilize the ROM computed for one of the load cases as long as the desired range of deflection is covered. The ROM may, however, be reformulated by including appropriate eigenmodes in the reduction subspace if the applied loading conditions result in a drastically different dynamic response which cannot be captured through an existing ROM.
- Dynamic response related to a specific eigenfrequency can only be captured correctly when the corresponding eigenmode shape is included in the reduction subspace.

In the subsequent sections, test cases are presented to assess the utility of the ROM and the updating algorithm.

4. Discussion of results

Three test cases are considered for verification of the approach: (1) comparison to full FE solution of a cantilever beam excited harmonically at the free end, (2) comparison to experimentally measured frequency response curves of a thin metal sheet under base excitation, (3) large scale model reduction of a composite wingbox structure.

4.1. Comparison to FE solution – test case 1

The cantilever beam described in [34,35] is analysed first using the ROM and the solution is compared to the full FE solution from MSC Nastran. The dimensions of the beam are: length $l = 0.6931$ m, cross-section width $b = 0.0254$ m, cross-section depth $d = 0.99$ mm. The material properties of the beam are: elastic modulus $E = 200$ GPa, and density $\rho = 7{,}800$ kg m^{-3}. The FE model is generated using beam elements and the structure is excited at the free end using a concentrated point load and assuming the excitation frequency equal to the first modal frequency. An initial eigenvalue analysis is conducted to compute the mode shapes and modal frequencies of the structure.

The 1st bending mode is found to be at 1.68 Hz. The excitation force is chosen to be 0.06 N and a mass proportional damping with a damping ratio of 0.0189 is applied such that the transverse deflection at the free end exceeds 50 % of the cantilever length and can with

certainty said to be in the geometrically nonlinear domain. The structure is modelled using 10 beam elements which results in 66 × 66 stiffness and mass matrices in the full FE model. The full FE solution reaches a steady state at approximately around 25 s. The ROM is also simulated for 50 s, however, to ensure clarity in the comparison only the final few seconds in the steady state of the simulation results is depicted in Fig. 3.

The ROM solution is obtained with two methods: first by utilizing constant ROM parameters throughout the analysis (K-N reduction) and second by updating the ROM parameters (henceforth denoted as UK-N reduction) according to the algorithm presented in Section 3.

The maximum amplitude of deflection in the transverse direction reaches approximately 52.45 % of the cantilever length, 0.364 m in absolute magnitudes, under the described loading conditions in a full FE solution. In comparison, the K-N reduction predicts a transverse deflection of 0.416 m which is a deviation of 14.4 %. The UK-N performs better and predicts the maximum transverse deflection to be 0.362 m which is an error of 0.56 %. Similarly, for in-plane displacements the FE solution results in 0.124 m, the K-N reduction predicts a deviation of 16.7 % and the UK-N predicts a difference of 0.4 %. It is notable that the linear analyses techniques are incapable of predicting these in-plane displacements, nor can they predict the geometric stiffening in the displacements.

The solution shows definite improvement when the UK-N is utilized with some additional computational costs in the offline stage. However, the UK-N is still more efficient than the full FE solution. For comparison, MSC Nastran completed the analysis in 298 s. The K-N analysis was completed in 4 s including all pre-processing computations. The UK-N required 28 s in total, however, the majority of this computation time was required for the preparatory nonlinear static analysis. The actual UK-N simulation required 7.6 s for completion. All computations were done on a Linux-PC with an Intel Xeon W-2145 CPU@ 3.7 GHz processor and 32 Gb RAM. It is notable that the ROM computations were executed using a 3 degrees of freedom (DOF) model which implies that the first three mode shapes were utilized to formulate the ROM. 200 load increments were utilized to construct the ROM database.

A convergence study was conducted by adding more eigenvectors in the reduction subspace to ensure that the ROM parameters did not significantly vary. Results of the convergence study for the UK-N are shown magnified in Fig. 4. It can be seen that the 1-DOF model results in a distinctly different response while utilizing two or higher number of eigenvectors in the reduction subspace results in responses with deviations in the order of 0.1 %.

4.2. Comparison to experimental results – test case 2

An experimental study for extremely large amplitude vibrations in cantilevers has been presented in [10] where the dynamic response of a thin steel sheet under base excitation was measured using a high-speed camera. The dimensions of the chosen test structure are described as: length $l = 81.5$ mm, width $b = 9$ mm and depth $d = 0.0762$ mm. The material properties are: elastic modulus $E = 200$ GPa and material density $\rho = 7{,}800$ kg m^{-3}. The first modal frequency computed using a linear eigenvalue analysis is found to be 9.38 Hz. The structure is excited with a force of 0.0005 N and a mass proportional damping is applied with a damping ratio 0.0068. A frequency sweep around the linear modal frequency is conducted and the peak amplitudes at each excitation frequency is captured to generate the frequency response curve. Both K-N and UK-N based analyses are conducted for comparison with the experimental results and to demonstrate the effect of the updating algorithm. The ROM is constructed using the first three eigenvectors in the reduction subspace. In case of the UK-N, 200 load increments are applied to construct the ROM database. In Fig. 5 the frequency response curves are compared to the experimental data for the transverse and in-plane displacements. The UK-N evidently performs better than the K-N approach. When utilizing the UK-N approach, a hardening type nonlinearity is perceivable at 80 % transverse tip deflection. In comparison, with the same analysis parameters, the K-N reduction significantly over-predicts the peak amplitudes and furthermore, is

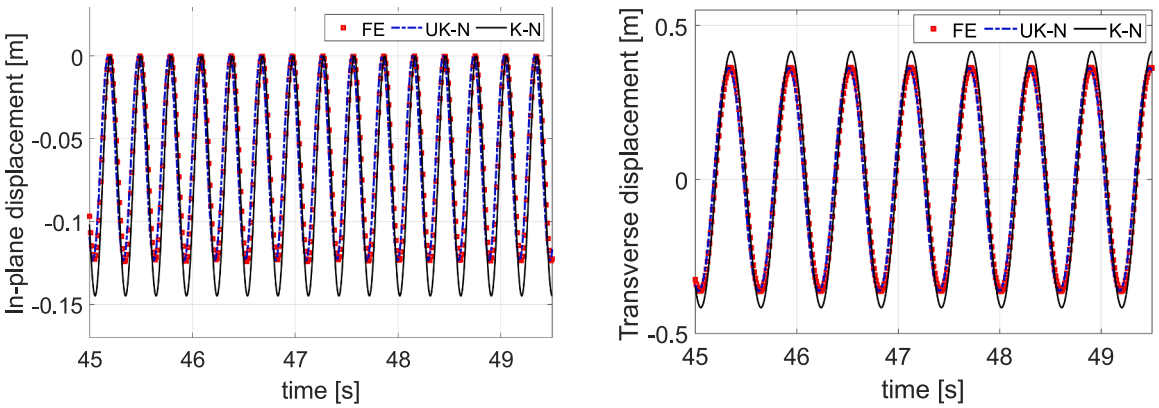

Fig 3. Comparison of time domain response of a steel cantilever beam $l = 0.6931$ m, $b = 0.0254$ m, $d = 0.99$ mm obtained using full FEM, K-N and UK-N reduction – (a) in-plane tip displacement, (b) transverse tip displacement.

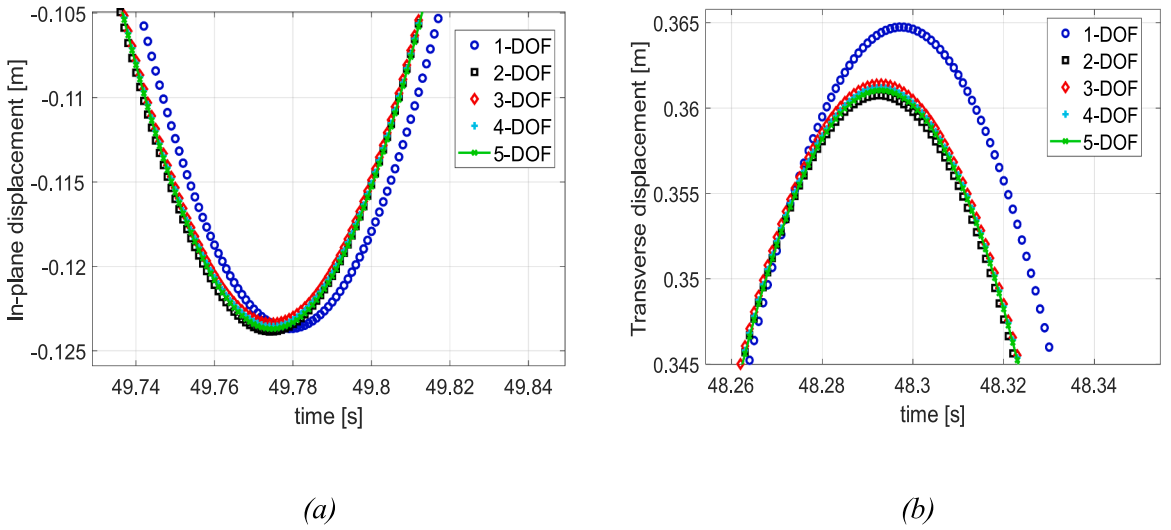

Fig 4. Magnified view of the time domain response of the steel cantilever beam $l = 0.6931$ m, $b = 0.0254$ m, $d = 0.99$ mm, obtained using various DOFs in the ROM for convergence analysis – (a) in-plane displacement, (b) transverse displacement.

ineffective in capturing the hardening nonlinearity. However, it is also evident that the experimental results show a greater degree of hardening effect than the UK-N predicts.

The deviation of the results is partially explainable through the discussions in Section 3 where it has been highlighted that to ensure efficiency in the analyses, the iterative corrector step is eliminated from the algorithm. This implies that at extremely large deflections, such as in this test case, the expected solution error is incrementally augmented with increasing deflections.

In Fig. 6, frequency response curves generated on the basis of the force corrected solution (corrected UK-N) are presented. This means that in each analysis step, it is ensured through a predictor-corrector approach that the internal forces and external forces are equivalent.

There is a noticeable difference in the corrected UK-N response which is closer to the experimental results, however, the corrected UK-N is akin to solving a full FE system and does not enable our objective of an efficient solution (in this example requiring over 8 h for completion). Additionally, the benefits of using a corrected solution are relatively small in comparison to the exponential increase in simulation time; especially within the domain of moderately large deflections up to 50 % transverse tip deflection. Therefore, for the subsequent analyses moderately large deflections are considered where the UK-N (with no force correction) performs sufficiently well in terms of accuracy and efficiency.

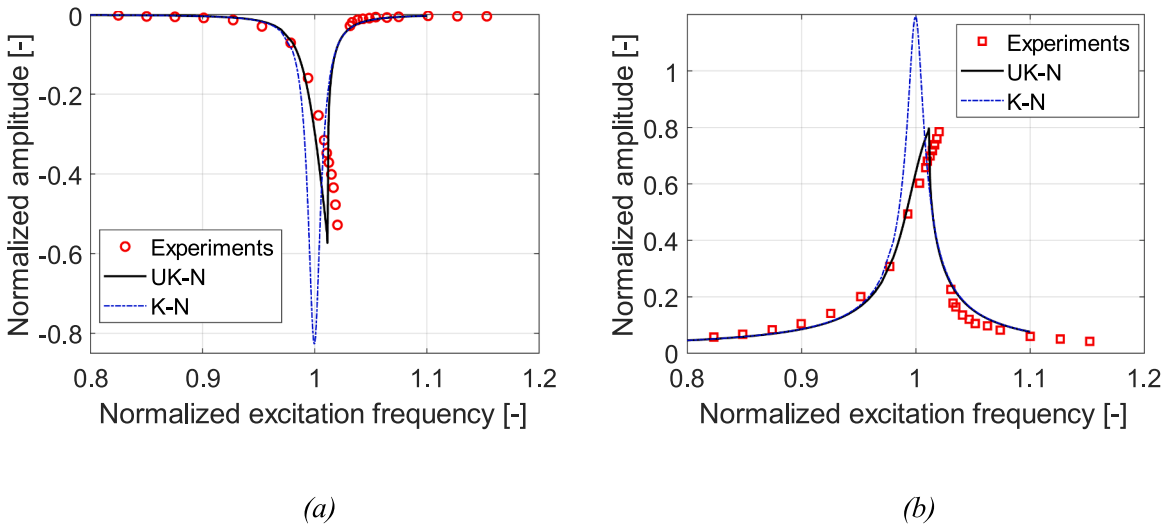

Fig 5. Comparison of K-N and UK-N based responses to experimental frequency response curves [10] of thin metal sheet $l = 81.5$ mm, $b = 9$ mm, $d = 0.0762$ mm – (a) in-plane displacement, (b) transverse displacement.

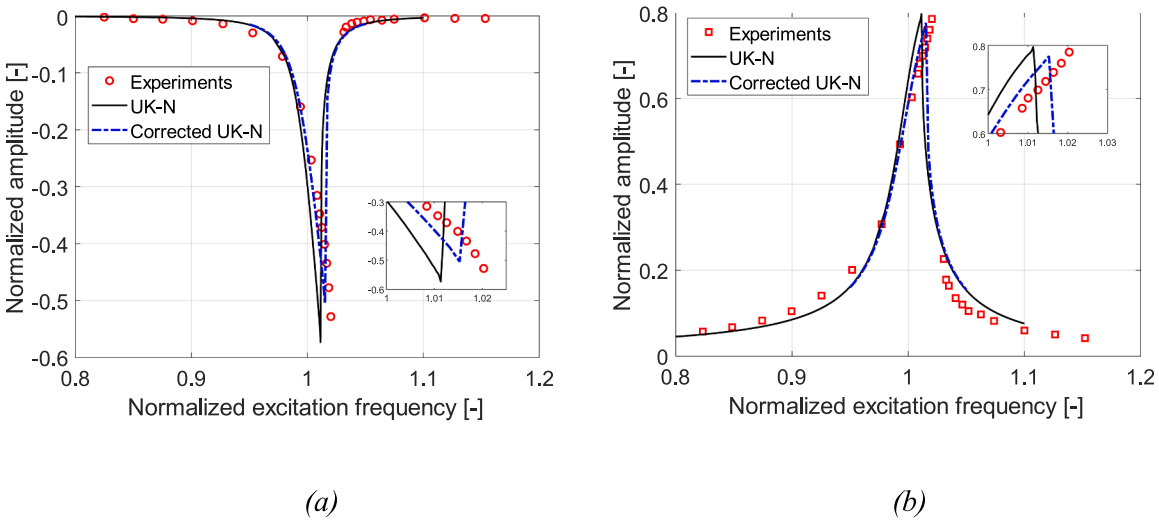

Fig 6. Comparison of the frequency response with a force corrected UK-N solution for a thin metal sheet $l = 81.5$ mm, $b = 9$ mm, $d = 0.0762$ mm – (a) in-plane displacement, (b) transverse displacement, magnified view of the peaks in the inset figure.

4.3. *Wingbox structure – test case 3*

The previous test cases demonstrate the potential for application of the K-N method through simple beam models. To further assess its applicability, we consider a slender wingbox structure designed to undergo large deflections when subjected to generic aircraft loads. The nonlinear static deflection behaviour of this wingbox was first presented in [26,36] and an adapted model was subsequently studied in [32]. The general construction of the wingbox is typical with an assembly of skin panels, spars and ribs. The entire model is constructed using only triangular shell elements [37] with anisotropic material description, where $G_{11} = G_{22} = 79.15$ GPa, $G_{12} = 26.91$ GPa and $G_{33} = 26.12$ GPa in the material property matrix. The wing spans across 20 m and a variable thickness distribution is defined across the span (see Fig. 7). For a detailed geometrical description and dimensions of the wingbox, the reader is referred to [26,32]. The FE model comprises 8660 elements and 4097 node points resulting in 24,582 degrees of freedom. The structure is sinusoidally excited at 0.685 Hz which lies in the neighbourhood of the first modal frequency. A concentrated force of 1,000 N is applied at the tip of the wingbox at two locations – 40 % and 60 % chord positions and the wing root is fully clamped along the cross-sectional profile grid

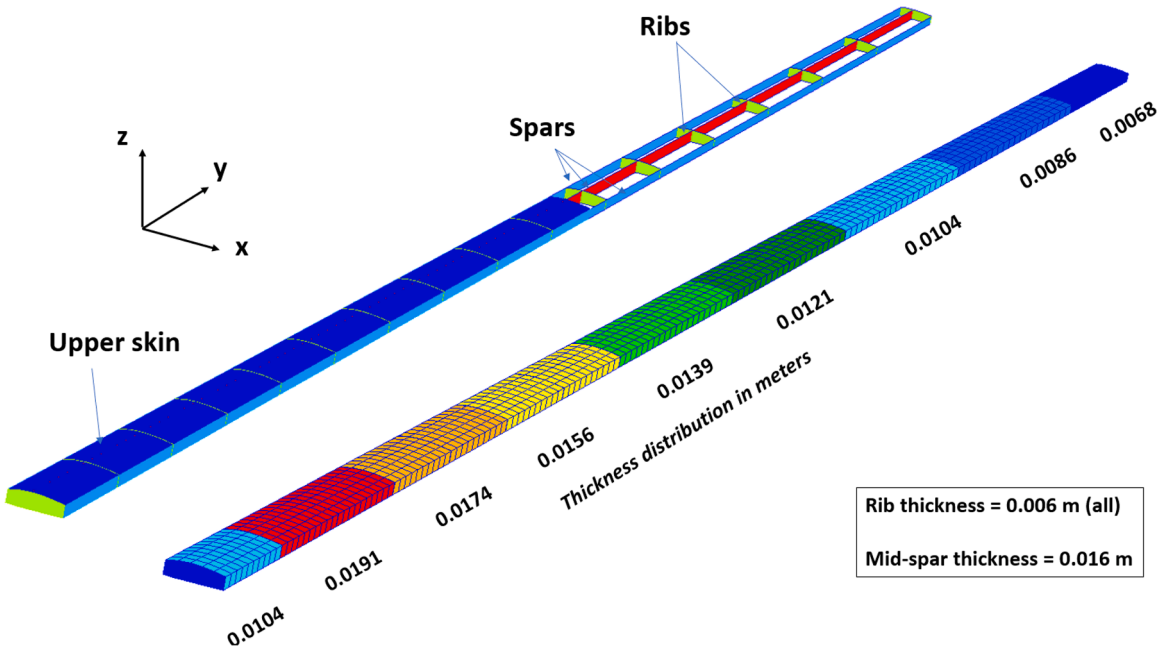

Fig 7. Wingbox construction and thickness distribution across the span.

points. A mass proportional damping is applied with a damping ratio 0.0562. The system is simulated for a total time of 30 s using an adaptive time increment in Nastran and a fixed time increment of 0.001 s in the UK-N analysis. A convergence study is conducted and the first 8 eigenmodes are selected for creating the reduced order model which results in an 8 DOF system.

In Fig. 8, a comparison of the in-plane and transverse displacements at the wingbox tip, obtained through the full FE solution in Nastran and the UK-N approach is shown. For clarity in the comparison, only 5 s of the simulation time in steady state are shown. The results agree very well with each other with a difference of 0.02 % in the transverse and 0.94 % in the in-plane displacements. The full FE solution in Nastran required 4.85 h for completion whereas the UK-N analysis with the 8 DOF model is fully executed in 4.16 mins which is a reduction of 98.6 % in the simulation time. However, since the FE model is large, the offline stage consumes significant computational effort for generating the ROM parameters.

The computational cost incurred in the offline stage is dependent on the number of force increments and model updates applied in the nonlinear static analyses. For smaller FE models, choosing a large number of increments automatically satisfies the requirements of the updating process. However, for larger models such as the wingbox structure, it is essential to assess the optimal number of model updates and force increments needed for the dynamic analyses to have a converged response. Alternately, specifying a randomly large number of increments would result in excess computational cost. A comparison of the variation in dynamic response with the increase in the number of ROM updates in the offline stage is shown in Fig. 9a. The maximum displacements, normalized by the FE solution, in the steady state is plotted against the number of ROM updates. The transverse displacements, in particular, converge rather quickly while a greater number of increments are required to obtain a convergence in the in-plane displacements. For the analysis presented here 100 increments were utilized which required a computational time of approximately 2.8 h. However, depending on the design stage i.e. early preliminary or detailed design, the user has the choice to use lesser number of increments with some compromise with the accuracy. In this example, the use of 40 increments is sufficient to obtain results with a maximum of 2 % error margin, as seen in Fig. 9a. In Fig. 9b, the time required in the offline stage is plotted against the number of ROM updates used. The variation is almost linear since each cycle of ROM update essentially performs the same set of computations with a different geometrical configuration. It is noted that the offline stage is required only once for any specific loading condition. Therefore, the gain in computational efficiency is increasingly greater when the ROM is utilized for multiple analyses, which is often an engineering necessity.

Finally, the nonlinear frequency response curves for the first two bending modes (in two perpendicular planes, *x*-*y* and *y*-*z* as seen in Fig. 7) of the wingbox model are presented in Fig. 10. To generate the curve, time domain nonlinear analyses are conducted at different excitation frequencies. The indicated forces in Fig. 10 are applied at two node points at the 40 % and 60 % chord locations.

At each excitation frequency, the maximum amplitude from the steady state response is captured. This is represented as a plot of the peak amplitudes normalized by the span of the wingbox against the absolute excitation frequencies. It is observed that the first mode does not show any significant frequency shifts even at large amplitudes when the tip deflections are over 50 % of the wing span. This is somewhat in agreement with the experimental results presented in [10] for the first bending mode where it is also seen that the frequency shifts are mild at extremely large amplitude of deflections. The frequency response for the second mode, however, shows a relatively stronger hardening effect already at 16 % tip deflection. Even though the general bending profiles are same for both mode shapes, the wingbox construction is not symmetrical about all axes and therefore some differences are expected in the bending behaviour in two different planes.

The ROM computations were significantly faster in generating the frequency response curves. It was possible to generate the entire curve in Fig. 10a, with 90 data points, using the ROM in 5.87 h. While each Nastran analysis at a single excitation frequency already requires nearly 5 h for completion and generating a similar curve with 90 data points, thus, would require over 2 weeks of simulation

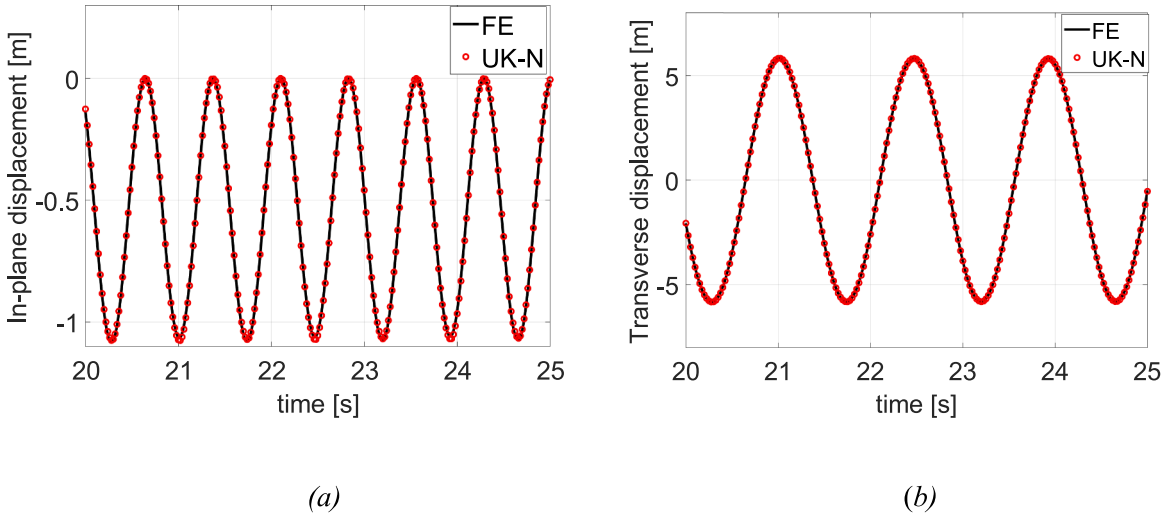

Fig 8. Comparison between UK-N and full FE time domain response at the free end of the composite wingbox -(a) in-plane displacement, (b) transverse displacement.

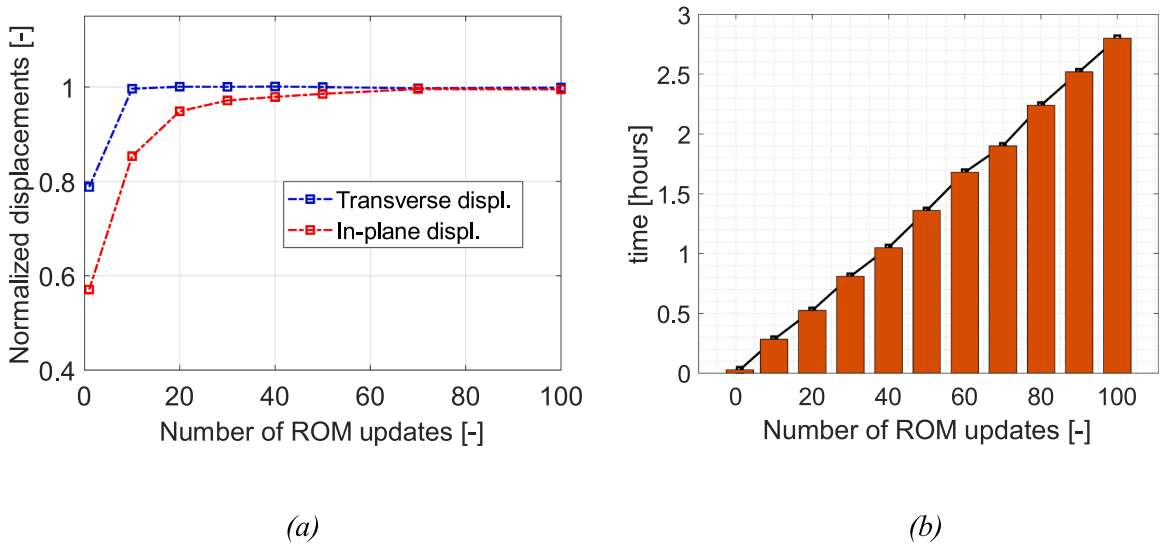

Fig 9. (a) Displacement convergence with increasing number of ROM updates in the offline stage, (b) increase in pre-processing time in the offline stage with number of ROM updates.

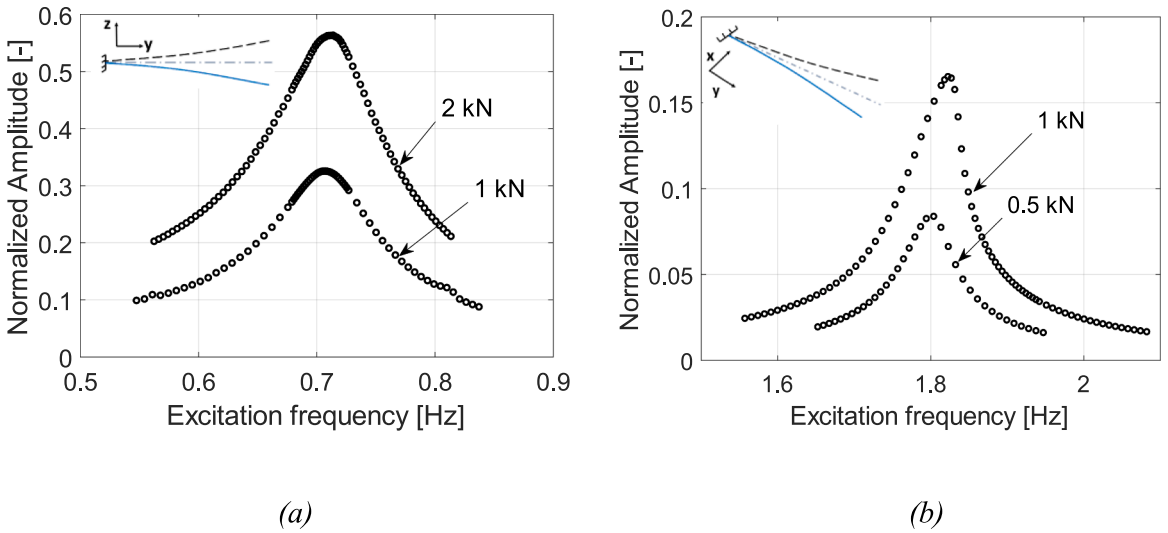

Fig 10. Nonlinear frequency response curves for the first two modes of the wingbox model – (a) Bending in the y-z plane, (b) Bending in the x-y plane.

time. The efficiency of the ROM can be further enhanced with the use of parametric continuation techniques.

5. Conclusions

The K-N reduction technique has been utilized for the first time to investigate nonlinear dynamics of cantilevers comprising large number of degrees of freedom. It has been found that the ROM based on K-N approach can predict the response of mildly nonlinear systems well. However, at larger deflections the errors increase. The utilization of a ROM updating algorithm (UK-N) has been proposed which perceptibly improves the performance of the K-N reduction. Comparison to experimental results at very large deflections demonstrate that although the UK-N performs significantly better, some deviations still exist from the experimental response which at least partially arise due to the lack of force correction in the iterative algorithms. Additionally, large scale model reduction is conducted on a composite wingbox structure to demonstrate potential applications in the aeronautical industry. It is concluded, based on the test cases studied, that UK-N is well suited for moderately large deflections of high aspect ratio cantilevers and generally outperforms full FE simulations in terms of efficiency with a reduction of up to 98 % in the simulation time. Up to 50 % reduction in the total time can be seen if the pre-processing time is considered. In cases where the analyses must be repeated several times, the benefits

of the ROM utilization are greater.

Funding

This research did not receive any specific grant from funding agencies in the public, commercial, or not-for-profit sectors.

CRediT authorship contribution statement

Kautuk Sinha: Writing – original draft, Validation, Software, Methodology, Investigation, Conceptualization. **Farbod Alijani:** Writing – review & editing, Supervision, Project administration, Methodology, Conceptualization. **Wolf R. Krüger:** Writing – review & editing, Supervision, Project administration, Conceptualization. **Roeland De Breuker:** Writing – review & editing, Supervision, Project administration, Conceptualization.

Declaration of competing interest

The authors declare that they have no known competing financial interests or personal relationships that could have appeared to influence the work reported in this paper.

Data availability

Data will be made available on request.

Appendix

The K-N reduction is independent of the element type used in the FE model. In this work, a planar beam element and a triangular shell element [37,38] were utilized. The quadratic (**Q**) and cubic (**C**) stiffness tensors are computed as higher order derivatives of the total in-plane strain energy of the system. The derivations are described in detail in [29-31].

A. *Beam element*

Strain and curvature of a planar beam element (Fig. A.1) in the finite element framework are defined in this section.

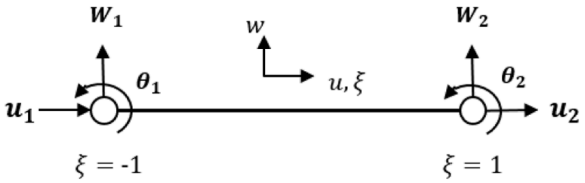

Fig A.1. Element degrees of freedom in the beam element.

The strain ε and the curvature χ for this element is defined as [29]:

$$\varepsilon = \frac{(u_2 - u_1)}{L} + \frac{1}{2}\left[\frac{(u_2 - u_1)^2}{L} + \frac{6}{5L^2}(w_1 - w_2)^2 + \frac{2}{15}(\theta_1 - \theta_2)^2 + \frac{1}{5}\theta_1\theta_2 + \frac{1}{5L}(\theta_1 + \theta_2)(w_1 - w_2)\right]$$

$$\chi = -\frac{1}{L^2}\left[3w_1 - 3w_2 - \frac{6w_1 x}{L} + \frac{6w_2 x}{L} + (2L - 3x)\theta_1 + (L - 3x)\theta_2\right]$$

The total strain energy of an element is then:

$$U_{elem} = \frac{1}{2}\,\mathrm{Al}_{elem}\,\varepsilon'\,E\,\varepsilon$$

The higher order derivatives of the strain energy then provide us with the following stiffness tensors required for the ROM computations:

$$L_{ij} = EAl_{elem}\left(\varepsilon\frac{\partial^2\varepsilon}{\partial q_i\,\partial q_j} + \frac{\partial\varepsilon}{\partial q_i}\,\frac{\partial\varepsilon}{\partial q_j}\right)$$

$$Q_{ijk} = \frac{EAl_{elem}}{2}\left(\frac{\partial\varepsilon}{\partial q_j}\,\frac{\partial^2\varepsilon}{\partial q_i\,\partial q_k} + \frac{\partial\varepsilon}{\partial q_i}\,\frac{\partial^2\varepsilon}{\partial q_j\,\partial q_k} + \frac{\partial\varepsilon}{\partial q_k}\,\frac{\partial^2\varepsilon}{\partial q_i\,\partial q_j}\right)$$

$$C_{ijkl} = \frac{EAl_{elem}}{6}\left(\frac{\partial^2\varepsilon}{\partial q_i\,\partial q_l}\,\frac{\partial^2\varepsilon}{\partial q_j\,\partial q_k} + \frac{\partial^2\varepsilon}{\partial q_j\,\partial q_l}\,\frac{\partial^2\varepsilon}{\partial q_i\,\partial q_k} + \frac{\partial^2\varepsilon}{\partial q_k\,\partial q_l}\,\frac{\partial^2\varepsilon}{\partial q_i\,\partial q_j}\right)$$

B. Shell Element

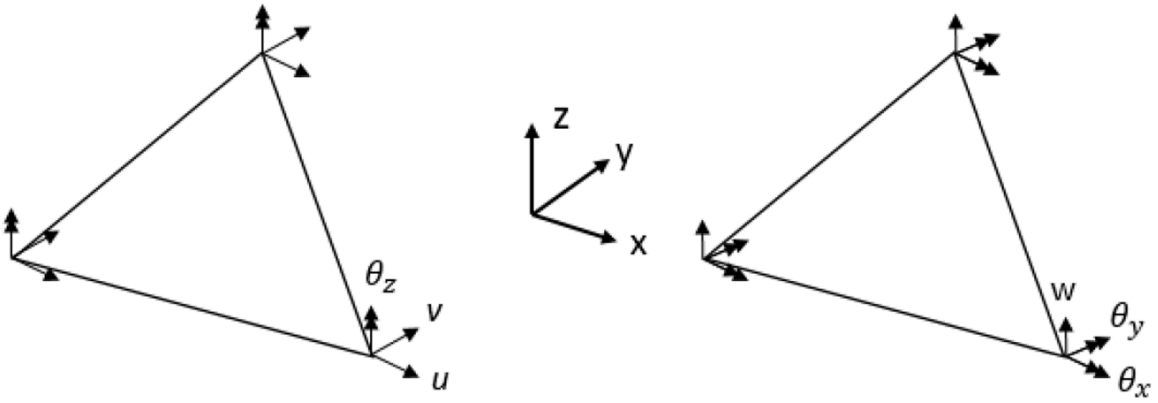

Fig B.1. Element degrees of freedom in the shell element.

The nonlinear strain of the shell element (Fig. B.1) is defined as:

$$\varepsilon = \varepsilon_l + \varepsilon_{nl} = \left(\mathbf{B_l} + \frac{1}{2}\,\mathbf{B_{nl}}(\mathbf{q})\right)\mathbf{q}$$

$$\mathbf{B_l} = \frac{1}{2A}\,[\mathbf{B}_1\ \mathbf{B}_2\ \mathbf{B}_3],$$

where A is the element area.

Considering that the three nodal coordinates are *(x1, y1), (x2, y2)* and *(x3, y3)*,

$$x_{ij} = x_i - x_j$$

$$x_{ij} = x_i - x_j$$

$$\mathbf{B}_1 = \begin{bmatrix} y_{23} & 0 & 0 & 0 & 0 & \dfrac{y_{23}(y_{13}-y_{21})}{6} \\ 0 & x_{23} & 0 & 0 & 0 & \dfrac{x_{32}(x_{32}-x_{12})}{6} \\ x_{32} & y_{32} & 0 & 0 & 0 & \dfrac{x_{31}y_{13}-x_{12}y_{21}}{3} \end{bmatrix}$$

$$\mathbf{B}_2 = \begin{bmatrix} y_{31} & 0 & 0 & 0 & 0 & \dfrac{y_{31}(y_{21}-y_{32})}{6} \\ 0 & x_{13} & 0 & 0 & 0 & \dfrac{x_{13}(x_{12}-x_{23})}{6} \\ x_{13} & y_{31} & 0 & 0 & 0 & \dfrac{x_{12}y_{21}-x_{23}y_{32}}{3} \end{bmatrix}$$

$$\mathbf{B}_3 = \begin{bmatrix} y_{12} & 0 & 0 & 0 & 0 & \dfrac{y_{12}(y_{32}-y_{13})}{6} \\ 0 & x_{21} & 0 & 0 & 0 & \dfrac{x_{21}(x_{23}-x_{31})}{6} \\ x_{21} & y_{12} & 0 & 0 & 0 & \dfrac{x_{23}y_{32}-x_{31}y_{13}}{3} \end{bmatrix}$$

The nonlinear strain component can be computed using the $\mathbf{B_{nl}}(\mathbf{q})$ term which is given by:

$$\mathbf{B}_{\mathrm{nl}}(\mathbf{q}) = \begin{bmatrix} \mathbf{q}^{\mathrm{t}}\,\mathrm{K}_{\mathrm{xx}} \\ \mathbf{q}^{\mathrm{t}}\,\mathrm{K}_{\mathrm{yy}} \\ \mathbf{q}^{\mathrm{t}}\,\mathrm{K}_{\mathrm{xy}} \end{bmatrix}$$

$$\mathrm{K}_{xx} = \mathbf{B}_w^t \mathbf{T}_x^t \mathbf{T}_x \mathbf{B}_w + \mathbf{B}_v^t \mathbf{T}_x^t \mathbf{T}_x \mathbf{B}_v$$

$$\mathrm{K}_{yy} = \mathbf{B}_w^t \mathbf{T}_y^t \mathbf{T}_y \mathbf{B}_w + \mathbf{B}_u^t \mathbf{T}_y^t \mathbf{T}_y \mathbf{B}_u$$

$$\mathrm{K}_{xx} = \mathbf{B}_w^t \left(\mathbf{T}_x^t \mathbf{T}_y + \mathbf{T}_y^t \mathbf{T}_x \right) \mathbf{B}_w$$

Here,

$$\mathbf{T}_x = \frac{1}{2\mathrm{A}} \begin{bmatrix} y_{23} & y_{31} & y_{12} \end{bmatrix} \text{ and } \mathbf{T}_y = \frac{1}{2\mathrm{A}} \begin{bmatrix} x_{32} & y_{13} & x_{21} \end{bmatrix}$$

The other terms involving $\mathbf{B}_{\mathrm{u}}$, $\mathbf{B}_{\mathrm{v}}$, $\mathbf{B}_{\mathrm{w}}$ are constant matrices consisting of 0 and 1. The explicit formulations of these matrices can be found in [39].

The in-plane strain energy is then described using the following equation:

$$U = \frac{1}{2} \mathrm{A} \mathscr{A}_m \left(\varepsilon_{l\alpha} + \varepsilon_{nl\alpha} \right) \left(\varepsilon_{l\beta} + \varepsilon_{nl\beta} \right), \ \alpha, \beta = 1 \textit{ to } 3$$

The stiffness tensors are then obtained as derivatives of the strain energy in a similar manner as described for the beam elements.

References

[1] K. Bisshopp, D. Drucker, Large deflection of cantilever beams, Q. Appl. Math. 3 (3) (1945) 272–275, https://doi.org/10.1090/qam/13360.
[2] M.R.M. Crespo da Silva, C.C. Glynn, Nonlinear flexural-flexural-torsional dynamics of inextensional beams. I. Equations of motion, J. Struct. Mech. 6 (4) (1978) 437–448, https://doi.org/10.1080/03601217808907348.
[3] M.R.M. Crespo da Silva, C.C. Glynn, Nonlinear flexural-flexural-torsional dynamics of inextensional beams. II. Forced motions, J. Struct. Mech. 6 (4) (1978) 449–461, https://doi.org/10.1080/03601217808907349.
[4] S.Nima Mahmoodi, Nader Jalili, Non-linear vibrations and frequency response analysis of piezoelectrically driven microcantilevers, Int. J. Non. Linear. Mech. 42 (4) (2007) 577–587, https://doi.org/10.1016/j.ijnonlinmec.2007.01.019.
[5] Seyed Nima Mahmoodi, Nader Jalili, Mohammed F. Daqaq, Modeling, nonlinear dynamics, and identification of a piezoelectrically actuated microcantilever sensor, IEEE/ASME Trans. Mechatron. 13 (1) (2008) 58–65, https://doi.org/10.1109/tmech.2008.915823.
[6] Juan C. Simo, Loc Vu-Quoc, A geometrically-exact rod model incorporating shear and torsion-warping deformation, Int. J. Solids. Struct. 27 (3) (1991) 371–393, https://doi.org/10.1016/0020-7683(91)90089-x.
[7] Loc Vu-Quoc, H. Deng, Galerkin projection for geometrically exact sandwich beams allowing for ply drop-off, J. Appl. Mech. 62 (1995) 479–488, https://doi.org/10.1115/1.2895955.
[8] Deng-Qing Cao, Robin W. Tucker, Nonlinear dynamics of elastic rods using the Cosserat theory: modelling and simulation, Int. J. Solids. Struct. 45 (2) (2008) 460–477, https://doi.org/10.1016/j.ijsolstr.2007.08.016.
[9] Hamed Farokhi, Mergen H. Ghayesh, Extremely large-amplitude dynamics of cantilevers under coupled base excitation, Eur. J. Mech.-A/Solids 81 (2020) 103953, https://doi.org/10.1016/j.euromechsol.2020.103953.
[10] Hamed Farokhi, Yiwei Xia, Alper Erturk, Experimentally validated geometrically exact model for extreme nonlinear motions of cantilevers, Nonlinear. Dyn. 107 (2022) 457–475, https://doi.org/10.1007/s11071-021-07023-9.
[11] Zhicun Wang, Ping C. Chen, Danny D. Liu, Dean T. Mook, Nonlinear-aerodynamics/nonlinear-structure interaction methodology for a high-altitude long-endurance wing, J. Aircr. 47 (2) (2010) 556–566, https://doi.org/10.2514/1.45694.
[12] Mayuresh J. Patil, Dewey H. Hodges, Carlos ES Cesnik, Nonlinear aeroelasticity and flight dynamics of high-altitude long-endurance aircraft, J. Aircr. 38 (1) (2001) 88–94, https://doi.org/10.2514/2.2738.
[13] Weihua Su, Carlos ES Cesnik, Dynamic response of highly flexible flying wings, AIAA J. 49 (2) (2011) 324–339, https://doi.org/10.2514/1.j050496.
[14] Yinan Wang, Andrew Wynn, Rafael Palacios, Nonlinear modal aeroservoelastic analysis framework for flexible aircraft, AIAA J. 54 (10) (2016) 3075–3090, https://doi.org/10.2514/1.j054537.
[15] Cristina Riso, Carlos ES Cesnik, Geometrically nonlinear effects in wing aeroelastic dynamics at large deflections, J. Fluids. Struct. 120 (2023) 103897, https://doi.org/10.1016/j.jfluidstructs.2023.103897.
[16] Hu-Nan Chu, George Herrmann, Influence of large amplitudes on free flexural vibrations of rectangular elastic plates, J. Appl. Mech. 23 (1956) 532–540, https://doi.org/10.1115/1.4011396.
[17] W. Han, M. Petyt, Geometrically nonlinear vibration analysis of thin, rectangular plates using the hierarchical finite element method—I: the fundamental mode of isotropic plates, Comput. Struct. 63 (2) (1997) 295–308, https://doi.org/10.1016/s0045-7949(96)00345-8.
[18] Ahmed K. Noor, Jeanne M. Peters, Reduced basis technique for nonlinear analysis of structures, AIAA Journal 18 (4) (1980) 455–462, https://doi.org/10.2514/3.50778.
[19] Farbod Alijani, Marco Amabili, Nonlinear vibrations of laminated and sandwich rectangular plates with free edges. Part 1: theory and numerical simulations, Compos. Struct. 105 (2013) 422–436, https://doi.org/10.1016/j.compstruct.2013.05.034.
[20] M. Amabili, H.R. Moghaddasi, Non-linear dynamics of cantilevered circular cylindrical shells with thickness stretch, containing quiescent fluid with small-amplitude sloshing, J. Sound. Vib. 571 (2024) 118052, https://doi.org/10.1016/j.jsv.2023.118052.
[21] Marc P. Mignolet, Adam Przekop, Stephen A. Rizzi, S.Michael Spottswood, A review of indirect/non-intrusive reduced order modeling of nonlinear geometric structures, J. Sound. Vib. 332 (10) (2013) 2437–2460.
[22] M. McEwan, J. Wright, Jonathan Cooper, A. Leung, A finite element/modal technique for nonlinear plate and stiffened panel response prediction, in: 19th AIAA Applied Aerodynamics Conference, 2001, p. 1595.
[23] Sergio R. Idelsohn, Alberto Cardona, A reduction method for nonlinear structural dynamic analysis, Comput. Methods Appl. Mech. Eng. 49 (3) (1985) 253–279, https://doi.org/10.1016/0045-7825(85)90125-2.
[24] Paolo. Tiso, Optimal second order reduction basis selection for nonlinear transient analysis." Modal Analysis Topics, in: Proceedings of the 29th IMAC, A Conference on Structural Dynamics 3, Springer New York, New York, NY, 2011, https://doi.org/10.1007/978-1-4419-9299-4_3, 2011.

[25] Shobhit Jain, Paolo Tiso, Johannes B. Rutzmoser, Daniel J. Rixen, A quadratic manifold for model order reduction of nonlinear structural dynamics, Comput. Struct. 188 (2017) 80–94, https://doi.org/10.1016/j.compstruc.2017.04.005.
[26] Markus Raimund Ritter, An Extended Modal Approach For Nonlinear Aeroelastic Simulations of Highly Flexible Aircraft Structures, Technische Universitaet Berlin (Germany), 2019, https://doi.org/10.2514/6.2016-1794.
[27] Polarit Apiwattanalunggarn, Steven W. Shaw, Christophe Pierre, Dongying Jiang, Finite-element-based nonlinear modal reduction of a rotating beam with large-amplitude motion, Journal of Vibration and Control 9 (3–4) (2003) 235–263, https://doi.org/10.1177/107754603030751.
[28] Shobhit Jain, George Haller, How to compute invariant manifolds and their reduced dynamics in high-dimensional finite element models, Nonlinear. Dyn. (2022) 1–34, https://doi.org/10.1007/s11071-021-06957-4.
[29] Ke Liang, Mostafa Abdalla, Zafer Gürdal, A Koiter-Newton approach for nonlinear structural analysis, Int. J. Numer. Methods Eng. 96 (12) (2013) 763–786, https://doi.org/10.1002/nme.4581.
[30] Ke Liang, Martin Ruess, Mostafa Abdalla, The Koiter–Newton approach using von Kármán kinematics for buckling analyses of imperfection sensitive structures, Comput. Methods Appl. Mech. Eng. 279 (2014) 440–468, https://doi.org/10.1016/j.cma.2014.07.008.
[31] Kautuk Sinha, Niels K. Singh, Mostafa M. Abdalla, Roeland De Breuker, Farbod Alijani, A momentum subspace method for the model-order reduction in nonlinear structural dynamics: theory and experiments, Int. J. Non. Linear. Mech. 119 (2020) 103314, https://doi.org/10.1016/j.ijnonlinmec.2019.103314.
[32] Kautuk Sinha, Farbod Alijani, Wolf R. Krüger, Roeland De Breuker, Koiter–Newton Based Model Reduction for Large Deflection Analysis of Wing Structures, AIAA Journal (2023) 1–10, https://doi.org/10.2514/1.j062514.
[33] Nathan M. Newmark, A method of computation for structural dynamics, Journal of the engineering mechanics 85 (3) (1959) 67–94, https://doi.org/10.1061/jmcea3.0000098.
[34] C. Pany, G.V. Rao, Calculation of non-linear fundamental frequency of a cantilever beam using non-linear stiffness, J. Sound. Vib. 256 (4) (2002) 787–790, https://doi.org/10.1006/jsvi.2001.4224.
[35] Hans. Wagner, Large-amplitude free vibrations of a beam, J. Appl. Mech. 32 (1965) 887–892, https://doi.org/10.1115/1.3627331.
[36] Markus Ritter, Carlos E. Cesnik, Large deformation modeling of a beam type structure and a 3D wingbox using an enhanced modal approach, in: 57th AIAA/ASCE/AHS/ASC Structures, Structural Dynamics, and Materials Conference, 2016, https://doi.org/10.2514/6.2016-1708.
[37] Carmelo Militello, Carlos A. Felippa, The first ANDES elements: 9-dof plate bending triangles, Comput. Methods Appl. Mech. Eng. 93 (2) (1991) 217–246, https://doi.org/10.1016/0045-7825(91)90152-v.
[38] Ken Alvin, Horacio M. de La Fuente, Bjørn Haugen, Carlos A. Felippa, Membrane triangles with corner drilling freedoms—I. The EFF element, Finite Elements in Analysis and Design 12 (3–4) (1992) 163–187, https://doi.org/10.1016/0168-874x(92)90033-9.
[39] Ke. Liang, Ph.D. Dissertation, Delft University of Technology, 2013.
[40] P. Belardinelli, M.K. Ghatkesar, U. Staufer, F. Alijani, Linear and non-linear vibrations of fluid-filled hollow microcantilevers interacting with small particles, Int. J. Non. Linear. Mech. 93 (2017) 30–40.